Acta Mechanica Solida Sinica, Vol. 29, No. 5, October, 2016 ISSN 0894-9166
Published by AMSS Press, Wuhan, China

Two Kinds Equal Frequency Circuits to Achieve Locally Resonant Band Gap of a Circular Plate Attached Alternately by Piezoelectric Unimorphs**

Longxiang Dai[1,2] **Hongping Hu**[1,2*] **Shan Jiang**[1,2] **Xuedong Chen**[3]

([1] *Department of Mechanics, Huazhong University of Science and Technology, Wuhan* 430074*, China*)
([2] *Hubei Key Laboratory for Engineering Structural Analysis and Safety Assessment, Huazhong University of Science and Technology, Wuhan* 430074*, China*)
([3] *State Key Laboratory of Digital Manufacturing Equipment and Technology, Huazhong University of Science and Technology, Wuhan* 430074*, China*)

Received 15 April 2015, revision received 25 July 2016

ABSTRACT A circular thin plate is proposed for vibration attenuation, which is attached alternately by annular piezoelectric unimorphs with resonant shunt circuits. Two kinds of equal frequency resonant shunt circuits are designed to achieve an integrated locally resonant (LR) band gap (BG) with a much smaller transmission factor: (1) the structure is arrayed periodically while the resonant shunt circuits are aperiodic; (2) the resonant shunt circuits are periodic while the structure is aperiodic. The transmission factor curve is calculated, which is validated by the finite element method. Dependences of the LR BG performance upon the geometric and electric parameters are also analyzed.

KEY WORDS band gap, locally resonant, periodic circular plate, equal frequency shunt circuit

I. Introduction

In recent years, there have been growing efforts to the study of phononic crystals (PCs). A PC is a composite consisting of two or more materials arranged periodically. The elastic waves can be modulated when propagating in the PCs. Consequently, the vibration and waves can be isolated or enormously attenuated in some frequency ranges, which are called band gaps (BGs)[1,2]. The BGs can be divided into two categories according to generation mechanism: Bragg scattering and locally resonant (LR)[3]. It implies that the PCs have good potential for application in vibration absorption or reduction for the machines.

Nevertheless, low-frequency vibration is always a hot and difficult issue in vibration isolation or absorption for the machines by the use of the PCs. There are at least three reasons. First of all, most environmental noise and mechanical vibration focus in low frequency range. Next, to bring about low-frequency Bragg BG means that a PC structure should have a big size, because the spatial modulation of elasticity must be of the same order as the wavelength. In other words, only high frequency Bragg BGs can be brought about by a PC in normal size, which are far beyond the vibration frequency. In

* Corresponding author. E-mail: huhp@hust.edu.cn

** Project supported by the National Natural Science Foundation of China (Nos. 11272126, 51435006, and 51421062), the Fundamental Research Funds for the Central Universities, HUST: 2016JCTD114 and 2015TS121, and the Research Fund for the Doctoral Program of Higher Education of China (No. 20110142120050).

addition, although low-frequency LR BGs can be produced by the PCs with small dimensions, each unit cell of the conventional LR PCs consists of a heavy core with a soft coat, which is equivalent to a mass-spring oscillator. Thus a lower resonance frequency can just be obtained by a heavier PC[3–5]. As a result, designing smaller and lighter PCs with low-frequency BGs is an ideal way to meet the demand of vibration isolation or absorption for the machines.

However, heavy mass-spring structures of the LR PCs can be replaced by light inductor-capacitor oscillators, which are composed of piezoelectric patches connected independently by a resonant shunt circuit. Beams attached by periodic arrays of piezoelectric patches connected by shunt circuits were studied to control the propagation of vibration[6–9]. These studies revealed that locally resonant BGs could be obtained when the same resonant shunt circuits were adopted. Besides, another significant advantage of the PCs with piezoelectric materials was found that their BGs could be adjusted by tuning circuits and their parameters synchronously[10–15]. Aperiodicity was also introduced in the shunt circuit parameters[16]. Recently, vibration of a plate was suppressed by periodic arrays of hybrid-shunted piezoelectric patches connected by resonant resistive/inductive circuit and negative impedance converter, respectively. An attenuation band with width of 500 Hz and attenuation rate of 19 dB was obtained[17]. In a study of a thin rectangular plate with piezoelectric patches, the location and attenuation constants of the Bragg gap was tuned by resistive shunts, while the internal resonances of resonant shunt system split the dispersion curves and formed a LR BG[18]. Apparently, the PCs with beam and rectangular plate structure have been extensively studied.

It is crucial to control and isolate micro vibration for precision semiconductor manufacturing equipment like lithography[19], highly precise instruments such as atomic force microscopes, and machine tools for ultra-high precision machining[20]. An ultra-precision motion platform (UPMP) is an essential component of all the above-mentioned mechanical devices. A circular plate is commonly chosen as a structure of the UPMP since it owns better dynamic characteristics than a rectangular plate, especially for the rotary motion. Accordingly, isolating vibration for circular plate has aroused increasing interest[21, 22]. The piezoelectric bimorphs are often introduced into a thin circular plate. It is because the plate has a planar neutral layer and its governing equation for the transverse vibration meets the Bessel equation in cylindrical coordinate. However, usually a smooth surface should be owned by the UPMP in order to facilitate the installation of the workpiece. Thus, only one of the two surfaces of the circular plate can be attached by piezoelectric patches. In an asymmetrically laminated plate with elastic and piezoelectric layers, the neutral layer is unknown in advance. The neutral layer is no longer planar and is also load dependent. Therefore, one cannot place axes on the neutral curve as a reference[23].

Accordingly, a thin circular plate periodically attached by annular piezoelectric unimorphs is considered. The emphasis is placed on studying the isolation on vertical vibration coming from the side of the circular plate. The electric field in the flexural piezoelectric unimorphs is analyzed using precise electric field method by taking into account a distribution of the electric field over the thickness, not as a constant[24].

It can be assumed that the plate consists of cells arrayed periodically in the radius direction. However, different cells have different equivalent capacitances since each piezoelectric unimorph has a distinct electrode area though with the same width. It is because that the electrode area of piezoelectric unimorph increases with radius. That is to say, the plate is not a periodic structure as usual, and the Bloch theorem is not applicable here. Considering its inherent aperiodicity, the frequency response function (FRF) would be an effective tool to describe BG for a PC of limited size structure in practical application.

To achieve a LR BG, one should make all shunt circuits own an equal resonance frequency. There are two methods for two different scenarios. On one hand, if the plate arrayed periodically by piezoelectric patches of the same width, one should adopt different inductances in shunt circuits due to the variation of capacitance in cells. On the other hand, if an equal inductance is used in resonant shunt circuits of all unit cells, one should make the piezoelectric unimorphs own an equal equivalent capacitance. We mainly discuss the first method since these two methods have much similarity in analysis.

The paper is organized in four sections. This introduction (§I) is followed by the formulation of the model of the circular thin plate attached with piezoelectric unimorphs (§II). Numerical examples are given in §III where the features of LR BG are discussed. The effects of model parameters on the BGs of the plate are also illustrated in this section. Finally, a summary is presented and some conclusions are drawn in §IV.

II. Configuration and Formulation of the Model

As illustrated in Fig.1, the periodic circular thin plate model is composed of N unit cells. Each unit cell is divided into two parts based on whether or not it has a piezoelectric unimorph: Part α is composed of pure elastic rings which are only made of metallic material, and Part β consists of a piezoelectric unimorph and a metal layer with the thicknesses of h_{p} and h_{m} respectively. R_0 , R and h denote the inner radius, outer radius and thickness of the whole plate, respectively. The thickness and width of a unit cell satisfy: $h = h_{\mathrm{p}} + h_{\mathrm{m}}$ and $a = a_1 + a_2$, where a_1 and a_2 are the widths of Part α and Part β respectively. The plate is simply supported at the edge by a fixture, which vibrates along the vertical direction harmonically with amplitude A at a certain frequency ω, and a concentrated mass m_0 is attached in the middle of the plate. Each piezoelectric unimorph is polarized along the z axis, with electrodes on its upper and lower surfaces connected by a circuit consisting of an inductor and a resistor. The circuit impedance of the nth unit cell is denoted by $Z^{(n)}$.

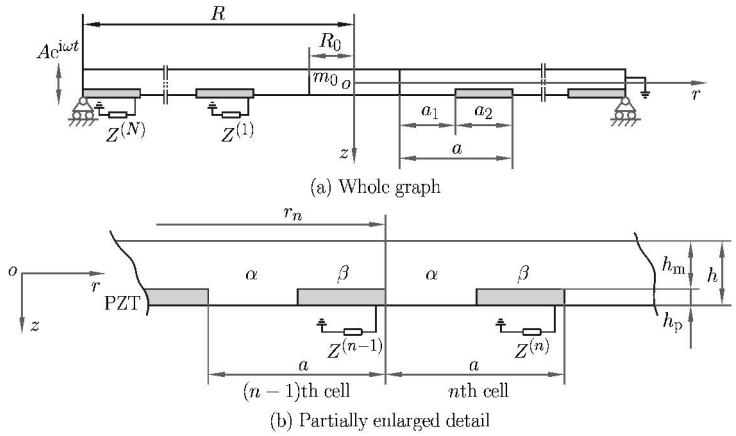

Fig. 1. Cross section of the plate.

2.1. Part α

For Part α, since the deflection is much smaller than the thickness of the plate and $R - R_0 \gg h$, and the bending of this Part is axisymmetric about the z axis, the deflection u_z has the following form:

$$u_z = u_z(r, t) \tag{1}$$

and the nontrivial components of strain are

$$S_{rr} = -z u_{z,rr}, \quad S_{\theta\theta} = -\frac{z}{r} u_{z,r} \tag{2}$$

where the convention that a comma followed by an index denotes the partial derivative of the corresponding variable applies.

The constitutive equations of the isotropic metallic material are

$$\begin{aligned} T_{rr} &= (\lambda + 2G) S_{rr} + \lambda S_{\theta\theta} + \lambda S_{zz} \\ T_{\theta\theta} &= \lambda S_{rr} + (\lambda + 2G) S_{\theta\theta} + \lambda S_{zz} \\ T_{zz} &= \lambda S_{rr} + \lambda S_{\theta\theta} + (\lambda + 2G) S_{zz} \end{aligned} \tag{3}$$

where the Lame's constants $\lambda = E\mu_{\mathrm{I}}/(1 + \mu_{\mathrm{I}})(1 - 2\mu_{\mathrm{I}})$, and $G = E/2(1 + \mu_{\mathrm{I}})$; E and μ_{I} are Young's modulus and Poisson's ratio of the metallic material, respectively. For a thin plate, Eq.(3) can be reduced by performing stress relaxation, i.e. $T_{zz} = 0$, as

$$\begin{aligned} T_{rr} &= Y_{\mathrm{I}} (S_{rr} + \mu_{\mathrm{I}} S_{\theta\theta}) \\ T_{\theta\theta} &= Y_{\mathrm{I}} (S_{\theta\theta} + \mu_{\mathrm{I}} S_{rr}) \end{aligned} \tag{4}$$

where $Y_{\mathrm{I}} = E/\left(1-\mu_{\mathrm{I}}^2\right)$. The bending moments and shearing force per unit length can be obtained from Eqs.(2) and (4) as

$$M_r = \int_{-h/2}^{h/2} T_{rr} z \mathrm{d}z = -K_{\mathrm{I}} \left(u_{z,rr} + \frac{\mu_{\mathrm{I}}}{r} u_{z,r} \right) \tag{5}$$

$$M_\theta = \int_{-h/2}^{h/2} T_{\theta\theta} z \mathrm{d}z = -K_{\mathrm{I}} \left(\mu_{\mathrm{I}} u_{z,rr} + \frac{1}{r} u_{z,r} \right) \tag{6}$$

$$Q_r = \int_{-h/2}^{h/2} T_{rz} \mathrm{d}z = M_{r,r} + \frac{M_r - M_\theta}{r} = -K_{\mathrm{I}} \left(\nabla^2 u_z \right)_{,r} \tag{7}$$

where $K_{\mathrm{I}} = Y_{\mathrm{I}} h^3/12$, and the Laplacian operation $\nabla^2 = \partial^2/\partial r^2 + \partial/(r\partial r)$.

The equation of motion of elastic rings is

$$Q_{r,r} + \frac{Q_r}{r} = m_{\mathrm{I}} \ddot{u}_z \tag{8}$$

where $m_{\mathrm{I}} = \rho_{\mathrm{I}} h$ is the mass per unit area of the elastic material, and ρ_{I} is the density of the elastic material. A superimposed dot represents the derivative with respect to time. Substituting Eq.(7) into Eq.(8) yields

$$-K_{\mathrm{I}} \nabla^2 \nabla^2 u_z = m_{\mathrm{I}} \ddot{u}_z \tag{9}$$

2.2. Part $\boldsymbol{\beta}$

For the asymmetrically laminated Part β with elastic and piezoelectric layers, we introduce a middle plane instead of a neutral axis[23]. The axes x_1 and x_2 of a coordinate (x_1, x_2, x_3) are placed in the geometric middle plane. Then the displacement field is approximated as

$$\begin{aligned} u_1(x_1, x_2, x_3, t) &= u_1^{(0)}(x_1, x_2, t) - x_3 u_{3,1} \\ u_2(x_1, x_2, x_3, t) &= u_2^{(0)}(x_1, x_2, t) - x_3 u_{3,2} \\ u_3(x_1, x_2, x_3, t) &= u_3(x_1, x_2, t) \end{aligned} \tag{10}$$

where $u_1^{(0)}$ and $u_2^{(0)}$ are the middle surface extensional displacements, and u_3 is the middle surface flexural displacement. The corresponding strains are

$$\begin{aligned} &S_1 = u_{1,1}^{(0)} - x_3 u_{3,11}, \quad S_2 = u_{2,2}^{(0)} - x_3 u_{3,22} \\ &S_{12} = u_{1,2}^{(0)} + u_{2,1}^{(0)} - 2x_3 u_{3,12} \end{aligned} \tag{11}$$

Letting the cylindrical coordinate $(r,\ \theta,\ z)$ correspond to (x_1, x_2, x_3), since the deformation of the plate is axisymmetric about the z axis, then $u_\theta^{(0)} = 0$ and $\partial/\partial\theta = 0$. In the cylindrical coordinate system, Eq.(11) can be recast as

$$S_{rr} = u_{r,r}^{(0)} - z u_{z,rr}, \quad S_{\theta\theta} = -\frac{z}{r} u_{z,r}, \quad S_{r\theta} = 0 \tag{12}$$

The constitutive equations for the piezoelectric material are[25]

$$\begin{aligned} T_{ij} &= c_{ijkl} S_{kl} - e_{kij} E_k \\ D_i &= e_{ikl} S_{kl} + \varepsilon_{ik} E_k \end{aligned} \tag{13}$$

where T_{ij} and S_{kl} are the mechanical stress and strain components, respectively, E_k is the electric field component, and D_i is the electric displacement component. Also, c_{ijkl}, e_{kij} and ε_{ki} denote the elastic, piezoelectric and dielectric constants, respectively.

The electric field, corresponding to the electrodes configuration in Fig.1, has the following components:

$$E_1 = E_2 = 0, \quad E_z = E_3 = -\varphi_{,3} \tag{14}$$

where φ is the electric potential across the piezoelectric layers. T_{rz}, $T_{z\theta}$ and $T_{r\theta}$ can be neglected by considering axially symmetrical deflection of the thin plate.

From Eqs.(13) and (14), the constitutive equations of Eq.(13) of the piezoelectric material poled in the z axis can be reduced to

$$\begin{aligned} T_{rr} &= c_{11}S_{rr} + c_{12}S_{\theta\theta} + c_{13}S_{zz} - e_{31}E_z \\ T_{\theta\theta} &= c_{12}S_{rr} + c_{11}S_{\theta\theta} + c_{13}S_{zz} - e_{31}E_z \\ T_{zz} &= c_{13}S_{rr} + c_{13}S_{\theta\theta} + c_{33}S_{zz} - e_{33}E_z \\ D_z &= D_3 = e_{31}S_{rr} + e_{31}S_{\theta\theta} + e_{33}S_{zz} + \varepsilon_{33}E_z \end{aligned} \tag{15}$$

Performing stress relaxation, i.e. $T_{zz} = 0$, on Eq.(15) yields

$$\begin{aligned} T_{rr} &= \bar{c}_{11}S_{rr} + \bar{c}_{12}S_{\theta\theta} - \bar{e}_{31}E_z \\ T_{\theta\theta} &= \bar{c}_{12}S_{rr} + \bar{c}_{11}S_{\theta\theta} - \bar{e}_{31}E_z \\ D_z &= \bar{e}_{31}(S_{rr} + S_{\theta\theta}) + \bar{\varepsilon}_{33}E_z \end{aligned} \tag{16}$$

where $\bar{c}_{11} = c_{11} - c_{13}^2/c_{33}$, $\bar{c}_{12} = c_{12} - c_{13}^2/c_{33}$, $\bar{e}_{31} = e_{31} - e_{33}c_{13}/c_{33}$, and $\bar{\varepsilon}_{33} = \varepsilon_{33} + e_{33}^2/c_{33}$. The electric displacement satisfies the Gaussian theorem of electrostatics

$$D_{z,z} = 0 \tag{17}$$

From Eqs.(12), $(14)_3$, $(16)_3$ and (17), the electric field component E_3 and electric potential of the piezoelectric unimorph can be solved as

$$\begin{aligned} E_z &= \frac{\bar{e}_{31}}{\bar{\varepsilon}_{33}}\left(u_{z,rr} + \frac{u_{z,r}}{r}\right)z - \frac{\bar{e}_{31}}{\bar{\varepsilon}_{33}}u_{r,r}^{(0)} + c_1 \\ \varphi &= -\int E_z \mathrm{d}z = -\frac{\bar{e}_{31}}{2\bar{\varepsilon}_{33}}\left(u_{z,rr} + \frac{u_{z,r}}{r}\right)z^2 + \left(\frac{\bar{e}_{31}}{\bar{\varepsilon}_{33}}u_{r,r}^{(0)} - c_1\right)z + c_2 \end{aligned} \tag{18}$$

where c_1 and c_1 are the integration constants independent of coordinate x_3. For piezoelectric unimorphs, the electrodes of $z = (h_\mathrm{m} - h_\mathrm{p})/2$ are regarded as zero voltage reference, i.e. $\varphi\left[(h_\mathrm{m} - h_\mathrm{p})/2\right] = 0$, thus the voltage on the electrodes of $z = (h_\mathrm{m} + h_\mathrm{p})/2$ is viewed as the output voltage, i.e. $\varphi\left[(h_\mathrm{m} + h_\mathrm{p})/2\right] = V$. From these two electric boundary conditions and $\mathrm{Eq.}(18)_2$, c_1 and c_2 can be solved as

$$\begin{aligned} c_1 &= -\frac{V}{h_\mathrm{p}} - \frac{h_\mathrm{m}}{2}\frac{\bar{e}_{31}}{\bar{\varepsilon}_{33}}\left(u_{z,rr} + \frac{u_{z,r}}{r}\right) + \frac{\bar{e}_{31}}{\bar{\varepsilon}_{33}}u_{r,r}^{(0)} \\ c_2 &= -\frac{h_\mathrm{m} - h_\mathrm{p}}{2}\frac{V}{h_\mathrm{p}} - \frac{h_\mathrm{m}^2 - h_\mathrm{p}^2}{8}\frac{\bar{e}_{31}}{\bar{\varepsilon}_{33}}\left(u_{z,rr} + \frac{u_{z,r}}{r}\right) \end{aligned} \tag{19}$$

Therefore, the precise electric field and electric displacement of piezoelectric unimorphs can be written as

$$\begin{aligned} E_z &= -\frac{V}{h_\mathrm{p}} + \frac{\bar{e}_{31}}{\bar{\varepsilon}_{33}}\left(u_{z,rr} + \frac{u_{z,r}}{r}\right)\left(z - \frac{h_\mathrm{m}}{2}\right) \\ D_z &= -\bar{\varepsilon}_{33}\frac{V}{h_\mathrm{p}} + \bar{e}_{31}u_{r,r}^{(0)} - \frac{\bar{e}_{31}h_\mathrm{m}}{2}\left(u_{z,rr} + \frac{u_{z,r}}{r}\right) \end{aligned} \tag{20}$$

The axial extensional force, the bending moments and the shearing force per unit length can be calculated from the combination of Eqs.(4), (12), (16) and (20) as

$$\begin{aligned} N_r = \int_{-h/2}^{h/2} T_{rr}\mathrm{d}z &= \bar{e}_{31}V + \left(Y_\mathrm{I}h_\mathrm{m} + \bar{c}_{11}h_\mathrm{p}\right)u_{r,r}^{(0)} \\ &+ \frac{Y_\mathrm{I}h_\mathrm{m}h_\mathrm{p}}{2}\left(u_{z,rr} + \frac{\mu_\mathrm{I}}{r}u_{z,r}\right) - \frac{1}{2}\bar{c}_{11}h_\mathrm{m}h_\mathrm{p}\left(u_{z,rr} + \frac{\mu_\mathrm{II}}{r}u_{z,r}\right) \end{aligned} \tag{21}$$

where $\mu_\mathrm{II} = \bar{c}_{12}/\bar{c}_{11}$. There are no radial load and radial constrain of the plate, therefore, the radial tension force satisfies

$$N_r = 0 \tag{22}$$

Then from Eqs.(21) and (22), we obtain

$$u_{r,r}^{(0)} = -k_1V - k_2\left(u_{z,rr} + \frac{\mu_\mathrm{I}}{r}u_{z,r}\right) + k_3\left(u_{z,rr} + \frac{\mu_\mathrm{II}}{r}u_{z,r}\right) \tag{23}$$

where

$$k_1=\frac{\bar{e}_{31}}{\xi},\quad k_2=\frac{Y_{\mathrm{I}}h_{\mathrm{m}}h_{\mathrm{p}}}{2\xi},\quad k_3=\frac{\bar{c}_{11}h_{\mathrm{m}}h_{\mathrm{p}}}{2\xi},\quad \xi=\bar{c}_{11}h_{\mathrm{p}}+Y_{\mathrm{I}}h_{\mathrm{m}}$$

The moments and shearing force are

$$\begin{aligned}M_r&=\int_{-h/2}^{h/2}T_{rr}z\mathrm{d}z\\&=\frac{1}{2}h_{\mathrm{m}}\bar{e}_{31}V+d_1u_{r,r}^{(0)}-d_2\left(u_{z,rr}+\frac{\mu_{\mathrm{I}}}{r}u_{z,r}\right)-d_3\left(u_{z,rr}+\frac{\mu_{\mathrm{II}}}{r}u_{z,r}\right)-d_4\left(u_{z,rr}+\frac{u_{z,r}}{r}\right)\end{aligned}\tag{24}$$

$$\begin{aligned}M_\theta&=\int_{-h/2}^{h/2}T_{\theta\theta}z\mathrm{d}z\\&=\frac{1}{2}Vh_{\mathrm{m}}\bar{e}_{31}+d_5u_{r,r}^{(0)}-d_2\left(\mu_{\mathrm{I}}u_{z,rr}+\frac{u_{z,r}}{r}\right)-d_3\left(\mu_{\mathrm{II}}u_{z,rr}+\frac{u_{z,r}}{r}\right)-d_4\left(u_{z,rr}+\frac{u_{z,r}}{r}\right)\end{aligned}\tag{25}$$

$$\begin{aligned}Q_r&=\int_{-h/2}^{h/2}T_{rz}\mathrm{d}z=M_{r,r}+\frac{M_r-M_\theta}{r}\\&=-\left(d_2+d_3+d_4\right)\left(\nabla^2u_z\right)_{,r}+d_5\left[\frac{k_1}{r}V+k_2\left(\frac{\mu_{\mathrm{I}}}{r^2}u_{z,r}+\frac{u_{z,rr}}{r}\right)-k_3\left(\frac{\mu_{\mathrm{II}}}{r^2}u_{z,r}+\frac{u_{z,rr}}{r}\right)\right]\\&\quad-d_1\left[\frac{k_1}{r}V+k_2\left(u_{z,rrr}+\frac{1+\mu_{\mathrm{I}}}{r}u_{z,rr}\right)-k_3\left(u_{z,rrr}+\frac{1+\mu_{\mathrm{II}}}{r}u_{z,rr}\right)\right]\end{aligned}\tag{26}$$

where

$$d_1=\frac{h_{\mathrm{m}}h_{\mathrm{p}}}{2}\left(\bar{c}_{11}-Y_{\mathrm{I}}\right),\quad d_2=Y_{\mathrm{I}}\left(\frac{h_{\mathrm{m}}^3}{12}+\frac{1}{4}h_{\mathrm{m}}h_{\mathrm{p}}^2\right),\quad d_3=\bar{c}_{11}\left(\frac{h_{\mathrm{p}}^3}{12}+\frac{1}{4}h_{\mathrm{m}}^2h_{\mathrm{p}}\right)$$
$$d_4=\frac{h_{\mathrm{p}}^3\bar{e}_{31}^2}{12\bar{\varepsilon}_{33}},\quad d_5=\frac{h_{\mathrm{m}}h_{\mathrm{p}}}{2}\left(\mu_{\mathrm{II}}\bar{c}_{11}-\mu_{\mathrm{I}}Y_{\mathrm{I}}\right)$$

The equation of motion of Part β is

$$Q_{r,r}+\frac{Q_r}{r}=m_{\mathrm{II}}\ddot{u}_z\tag{27}$$

where $m_{\mathrm{II}}=\rho_{\mathrm{I}}h_{\mathrm{m}}+\rho_{\mathrm{II}}h_{\mathrm{p}}$ is the mass per unit area of Part β and ρ_{II} is the density of the piezoelectric material.

Substituting Eq.(26) into Eq.(27) yields

$$\begin{aligned}&\left[f_1-\left(d_2+d_3+d_4\right)\right]u_{z,rrrr}+\left[f_1-\left(d_2+d_3+d_4\right)\right]\frac{2}{r}u_{z,rrr}\\&\quad-\left[f_2-\left(d_2+d_3+d_4\right)\right]\frac{1}{r^2}u_{z,rr}+\left[f_2-\left(d_2+d_3+d_4\right)\right]\frac{1}{r^3}u_{z,r}=m_{\mathrm{II}}\ddot{u}_z\end{aligned}\tag{28}$$

where

$$f_1=\frac{h_{\mathrm{m}}^2h_{\mathrm{p}}^2\left(Y_{\mathrm{I}}-\bar{c}_{11}\right)^2}{4\xi},\quad f_2=\frac{h_{\mathrm{m}}^2h_{\mathrm{p}}^2\left(\mu_{\mathrm{I}}Y_{\mathrm{I}}-\mu_{\mathrm{II}}\bar{c}_{11}\right)^2}{4\xi}$$

Equation (28) is a differential equation with variable coefficients, and it is difficult to obtain its analytic solution. Therefore, we adopt an approximate calculation method[26]. At first, Part β in an arbitrary nth unit cell is equally divided into N_1 infinitesimal elements along the radial direction. In each element, the radius of midpoint is approximately taken as the value of r in the coefficients since the elements size is sufficiently small to make the solution converge. Thus Eq.(28) is transformed into a differential equation with constant coefficients, which make it easy to obtain the solution.

2.3. Equal frequency circuit

The charge on the electrode of the piezoelectric unimorph of the nth unit cell is

$$Q_e^{(n)} = \sum_{k=1}^{N_1} \int_{A_k} D_3 \left(z = h/2\right) \mathrm{d}A_k \tag{29}$$

where the superscript (n) denotes the nth unit cell, and A_k is the area of the kth infinitesimal element in the nth unit cell. The current flowing out of the electrode is

$$I^{(n)} = -\dot{Q}_e^{(n)} \tag{30}$$

The output voltage and current meet the Ohm's law

$$I^{(n)} = \frac{V^{(n)}}{Z^{(n)}} \tag{31}$$

where $Z^{(n)} = \mathrm{i}\omega L^{(n)} + R^{(n)}$, with the imaginary unit 'i $= \sqrt{-1}$', since the circuit of the nth unit cell is composed of an inductor $L^{(n)}$ and a resistor $R^{(n)}$.

For an arbitrary nth unit cell, the equivalent static capacitance $C_{\mathrm{p}}^{(n)}$ of the piezoelectric unimorph and the circuit inductor $L^{(n)}$ constitute an electromagnetic oscillator. The resonant frequency $f_r^{(n)}$ of the oscillator can be estimated as

$$f_r^{(n)} = \frac{1}{2\pi} \sqrt{\frac{1}{L^{(n)} C_{\mathrm{p}}^{(n)}}} \tag{32}$$

where $C_{\mathrm{p}}^{(n)} = \pi \bar{\varepsilon}_{33} \left[2\left(R_0 + na\right) - a_2\right] a_2 / h_{\mathrm{p}}$. Hence, $C_{\mathrm{p}}^{(n)}$ varies with the number of unit cells if the plate is arrayed periodically in the geometric structure. As can be further known from Eq.(32), different unit cells have different resonant frequencies if the inductors in the circuits of unit cells have an equal inductance. Consequently, it is necessary to design equal frequency resonant shunt circuits for the periodic circular plate to achieve a LR BG. In order to make all unit cells have an equal resonant frequency, the inductance of the nth unit cell needs to be

$$L^{(n)} = \frac{2R - a_2}{2\left(R_0 + na\right) - a_2} L_0 \tag{33}$$

where $n = 1, 2, 3, \ldots, N$. The outer radius of the plate $R = R_0 + Na$. L_0 is chosen as a basic inductance, which is equal to inductance $L^{(N)}$ of the outermost unit cell.

2.4. General solutions

When the time-harmonic motion reaches the steady state, all fields are with the same time dependence, and the $\mathrm{e}^{\mathrm{i}\omega t}$ factor can be dropped. Therefore, we have the complex notation

$$\left\{u_z,\ V^{(n)},\ Q_e^{(n)},\ I^{(n)}\right\} = \mathrm{Re}\left\{\left[U_z,\ \bar{V}^{(n)},\ \bar{Q}_e^{(n)},\ \bar{I}^{(n)}\right] \mathrm{e}^{\mathrm{i}\omega t}\right\} \tag{34}$$

Then the governing equations of Eq.(9) become

$$K_{\mathrm{I}} \nabla^2 \nabla^2 U_z = \omega^2 m_{\mathrm{I}} U_z \tag{35}$$

The general solutions to Eq.(35) are

$$U_z = A_1^{(n)} J_0\left(\alpha_{\mathrm{I}} r\right) + A_2^{(n)} I_0\left(\alpha_{\mathrm{I}} r\right) + A_3^{(n)} Y_0\left(\alpha_{\mathrm{I}} r\right) + A_4^{(n)} K_0\left(\alpha_{\mathrm{I}} r\right) \tag{36}$$

where $\alpha_{\mathrm{I}}^4 = m_{\mathrm{I}}\omega^2 / K_{\mathrm{I}}$; $A_i^{(n)}$ (i =1, 2, 3, 4) are undetermined constants for Part α of the nth unit cell; J_0 and Y_0 are zero-order Bessel functions of the first kind and the second kind, respectively; and I_0 and K_0 are modified zero-order Bessel functions of the first kind and the second kind, respectively.

Similarly, Eq.(28) can be rewritten as

$$U_{z,rrrr} + \frac{2}{r} U_{z,rrr} - \frac{g_0}{r^2} U_{z,rr} + \frac{g_0}{r^3} U_{z,r} - g_1 U_z = 0 \tag{37}$$

where $g_0 = (d_2 + d_3 + d_4 - f_2)/(d_2 + d_3 + d_4 - f_1)$, and $g_1 = m_{\mathrm{II}}\omega^2/(d_2 + d_3 + d_4 - f_1)$. For an infinitesimal element, Eq.(37) is transformed into a differential equation with constant coefficients using the above-mentioned method. Thus for the kth infinitesimal element in the nth unit cell, the solution to Eq.(37) is

$$U_z = \sum_{j=1}^{4} B_{jk}^{(n)} \mathrm{e}^{\lambda_{jk} r} \quad (k = 1, 2, 3, \ldots, N_1) \tag{38}$$

where $B_{jk}^{(n)}$ $(j = 1, 2, 3, 4)$ are undetermined constants, and λ_{jk} $(j = 1, 2, 3, 4)$ are characteristic roots of the differential equation with constant coefficients.

2.5. Continuity and boundary conditions

It is necessary to satisfy the boundary conditions at both end edges and the continuity conditions inside the plates for the solutions in Eqs.(36) and (38). Inside Part β of an arbitrary nth unit cell, the continuity conditions between two adjacent infinitesimal elements are

$$\begin{aligned} &U_z^{(n)_\beta}\left(r_{n(k-1)}^{+}\right) = U_z^{(n)_\beta}\left(r_{nk}^{-}\right), \quad U_{z,r}^{(n)_\beta}\left(r_{n(k-1)}^{+}\right) = U_{z,r}^{(n)_\beta}\left(r_{nk}^{-}\right) \\ &M_r^{(n)_\beta}\left(r_{n(k-1)}^{+}\right) = M_r^{(n)_\beta}\left(r_{nk}^{-}\right), \quad Q_r^{(n)_\beta}\left(r_{n(k-1)}^{+}\right) = Q_r^{(n)_\beta}\left(r_{nk}^{-}\right) \end{aligned} \tag{39}$$

where $k = 2, 3, 4, \ldots, N_1$; the superscripts '+' and '−' denote the right and left ends of the element, respectively. From Fig.1, Part α and Part β within the nth unit cell are connected at $r = r_n + a_1$. Thus the displacement, the deflection angle, the bending moment and the shearing force satisfy the continuity conditions

$$\begin{aligned} &U_z^{(n)_\alpha}(r_n + a_1) = U_z^{(n)_\beta}(r_n + a_1), \quad U_{z,r}^{(n)_\alpha}(r_n + a_1) = U_{z,r}^{(n)_\beta}(r_n + a_1) \\ &M_r^{(n)_\alpha}(r_n + a_1) = M_r^{(n)_\beta}(r_n + a_1), \quad Q_r^{(n)_\alpha}(r_n + a_1) = Q_r^{(n)_\beta}(r_n + a_1) \end{aligned} \tag{40}$$

In addition, the continuity conditions between two adjacent unit cells, such as the $(n-1)$th and the nth unit cells, are

$$\begin{aligned} &U_z^{(n-1)_\beta}(r_n) = U_z^{(n)_\alpha}(r_n), \quad U_{z,r}^{(n-1)_\beta}(r_n) = U_{z,r}^{(n)_\alpha}(r_n) \\ &M_r^{(n-1)_\beta}(r_n) = M_r^{(n)_\alpha}(r_n), \quad Q_r^{(n-1)_\beta}(r_n) = Q_r^{(n)_\alpha}(r_n) \end{aligned} \tag{41}$$

Since the plate is attached by a concentrated mass at $r = R_0$, and is simply supported at the edge where $r = R$, the boundary conditions are respectively

$$\begin{aligned} &U_{z,r}^{(1)_\alpha}(R_0) = 0 \\ &2\pi R_0 K_{\mathrm{I}}\left(\nabla^2 U_z^{(1)_\alpha}\right)_{,r}\Big|_{r=R_0} = \omega^2 m_0 U_z^{(1)_\alpha}(R_0) \\ &U_z^{(N)_\beta}(R) = A \\ &\left(\frac{1}{2}h_{\mathrm{m}}\bar{e}_{31} - d_0 k_1\right)\bar{V}^{(N)} - (d_0 k_2 + d_2)\left[U_{z,rr}^{(N)_\beta}(R) + \frac{\mu_{\mathrm{I}}}{R}U_{z,r}^{(N)_\beta}(R)\right] \\ &\quad + (d_0 k_3 - d_3)\left[U_{z,rr}^{(N)_\beta}(R) + \frac{\mu_{\mathrm{II}}}{R}U_{z,r}^{(N)_\beta}(R)\right] - d_4\left[U_{z,rr}^{(N)_\beta}(R) + \frac{1}{R}U_{z,r}^{(N)_\beta}(R)\right] = 0 \end{aligned} \tag{42}$$

There are $4(4N_1 + 4)N$ linear equations in Eqs.(40), (41) and (42), which can determine $4N$ unknowns $A_i^{(n)}$ and $4NN_1$ unknowns $B_{jk}^{(n)}$. Subsequently, the deflection at the center of the plate, i.e. $r = R_0$, can be obtained. In order to measure the performance of the plate in attenuating the amplitude of elastic wave propagation, the transmission factor is defined as

$$T_f = 20\lg\left|\frac{U_z^{(N)_\beta}(R_0)}{U_z^{(1)_\alpha}(R)}\right| \tag{43}$$

The vibration can be attenuated in some frequency bands where the transmission factors are less than zero. Among these bands, apart from the locally resonant (LR) band gap (BG) and the Bragg BG, there also exist other frequency bands of vibration attenuation, which are named as the vibration attenuation band (VAB).

III. Numerical Results and Discussion

For the periodic circular thin plate shown in Fig.1, PZT-5H is chosen as the material for piezoelectric unimorphs, and Aluminum for metallic plates. For Aluminum, Young's modulus $E = 70$ GPa, Poisson's ratio $\mu_{\rm I} = 0.3$ and density $\rho_{\rm I} = 2700$ kg/m^3. While for PZT-5H, density $\rho_{\rm II} = 7500$ kg/m^3 and other material properties are listed below[27]:

$$c_{11} = 12.6, \quad c_{12} = 7.95, \quad c_{13} = 8.41, \quad c_{33} = 11.7 \times 10^{10}\ \text{N/m}^2, \quad e_{31} = -6.5$$
$$e_{33} = 23.3\,\text{C/m}^2, \quad \varepsilon_{33} = 1470\varepsilon_0, \quad \varepsilon_0 = 8.854 \times 10^{-12}\,\text{F/m}.$$

We set $h = 0.4$ mm, $h_{\rm p} = 0.1$ mm, $R_0 = 25$ mm, $N = 4$, and the acceleration amplitude of the input vibration $\omega^2 A = 1$ m/s^2 in all calculation. The widths $a = 20$ mm, $a_1 = 10$ mm, the concentrated mass $m_0 = 7.7$ g, and the resistance of each load circuit $R^{(n)} = 5\,\Omega$ are fixed unless otherwise stated.

To verify the theoretical model, the Frequency Response Function (FRF) curves, i.e. transmission factor versus frequency, which are obtained by theoretical calculation and the Finite Element Method (FEM) carried on the ANSYS software, respectively, are compared in Fig.2, where the basic inductance $L_0 = 0.02$ H is used. The results of the theoretical calculation agree well with those obtained from the FEM, especially when the frequency is below 1000 Hz. The increasing difference between the two curves above 1000 Hz results from ignoring the shearing deformation in the theoretical calculation. It also shows that there exists no obvious Bragg BGs within the frequency range between 0 and 3 kHz. It is because the size of structure is not big enough to obtain a Bragg BG of low frequency. Vibration isolation is focused on low frequency due to its importance and difficulty. The theoretical results are only demonstrated in the following discussion due to the high efficiency of calculation.

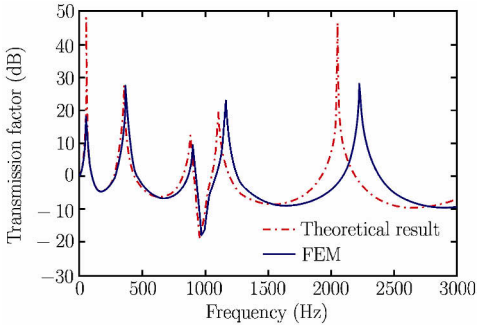

Fig. 2. FRF curves calculated by theoretical model and the FEM, respectively.

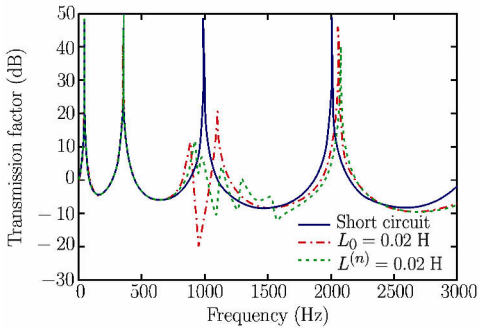

Fig. 3. FRF curves for different load circuits, where $R = 5\,\Omega$ is fixed.

The necessity of equal frequency resonant shunt circuits in achieving LR gap is then investigated. Figure 3 shows the FRF curves of three kinds of shunt circuits. It can be seen that only VABs occur when the circuits of all unit cells are shorted, which are caused by the periodic material arrangement due to the lack of electromagnetic oscillators. In the case that inductance $L^{(n)}$ of each unit cell is 0.02 H, there appear 4 additional LR gaps with minus transmission factor corresponding to the resonant frequency of the oscillators. It should be noted that the differences among them result from the unequal capacitance $C_{\rm p}^{(n)}$ of each unit cell. Finally, when equal frequency resonant shunt circuits are obtained by tuning inductance of each unit cell to satisfy Eq.(33), where $L_0 = 0.02$ H, an integrated LR gap is achieved with a much smaller transmission factor, -20 dB. It can be seen that the frequency (964 Hz), where the minimum transmission factor of the integrated gap locates, is lower than the resonant frequency (1068 Hz) obtained by Eq.(32). It is because that only the static capacitance in Eq. (32) is adopted, but in fact the capacitances include static and motional ones when the plate is vibrating. The motional capacitance depends on the driving frequency, while the static capacitance does not[28].

Then the effect of the parameters of equal frequency resonant shunt circuits on the integrated LR BG is discussed. Firstly, as shown in Fig.4, the FRF curves for different basic inductances, the integrated LR BG can be tuned by the inductances, where $L_0 = 0.02, 0.035, 0.05$ H. It is found that the variation of the inductance barely affects the VABs, especially for those far away from the LR BG. However, the

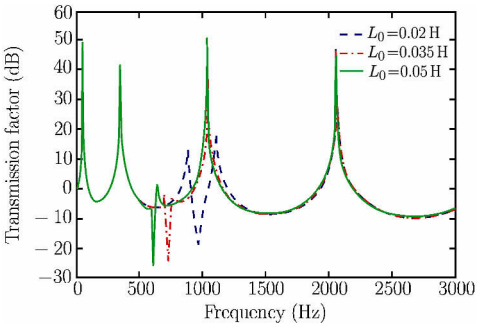

Fig. 4. FRF curves for different basic inductances.

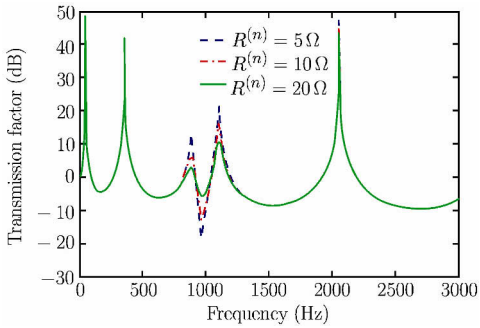

Fig. 5. FRF curves for different resistances.

center frequency as well as the width of the LR BG decreases with the increase of the inductance. It indicates that tuning an integrated LR BG is simply needed by adjusting the inductances, rather than reconfiguring the structure.

The effect of resistance on the BGs is further investigated. Figure 5 illustrates the FRF curves for different resistances, where $R^{(n)} = 5$, 10, 20 Ω, respectively, and the basic inductance $L_0 = 0.02$ H is fixed. It's clear that the increase of resistance dramatically increases the transmission factor of the LR BG, while the center frequency of the LR BG keeps unchanged. What's more, it should be noted that the transmission factor of peaks on both sides of the LR BG decreases with the increase of resistance. To further investigate the impact of resistance on peaks of the LR BG, the curves of transmission factor versus resistance for specific peak frequencies are plotted in Fig.6. The frequencies of 883, 964 and 1109 Hz correspond to the left, center and right peak frequencies of the LR BG, respectively. Clearly, if an optimum resistance is adopted, the appropriate transmission factors on the center frequency as well as on the two-side peak frequencies of the LR BG can be obtained.

Furthermore, we study the influence of structural or geometric parameters on vibration transmission by fixing the circuit parameters, such as the basic inductance $L_0 = 0.02$ H and resistances $R^{(n)} = 5\,\Omega$. The dependence of FRF curves on concentrated mass m_0 is shown in Fig.7, where $m_0 = 7.7$ g, 15.4 g, and 23.1 g, respectively. The curves indicate that the attenuation in VABs is strengthened and its center frequency decreases when the concentrated mass m_0 increases. However, it should also be pointed out that the change of concentrated mass almost has no influence upon the LR BG.

The impact of width ratio a_2/a of Part β to the whole unit cell on the FRF curves is shown in Fig.8, where $L_0 = 0.02$ H is fixed. Frequency of the LR BG decreases with the increase of a_2/a. The reason is that the capacitance $C_{\mathrm{p}}^{(n)}$ increases with the increase of width ratio a_2/a, and it leads to the decline of the resonant frequency $f_r^{(n)}$ of the oscillators, which can be known from Eq.(32). It is similar to the effect of increasing inductances on the LR BG frequency, as is shown in Fig.4. Moreover, the increase of width ratio a_2/a softens stiffness of the whole structure, which results in the decreasing frequency of the VABs.

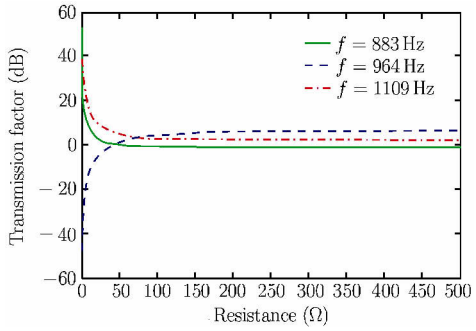

Fig. 6. Transmission factor versus resistance for different frequencies, where $m_0 = 7.7$ g, $L_0 = 0.02$ H, $a_2/a = 0.5$.

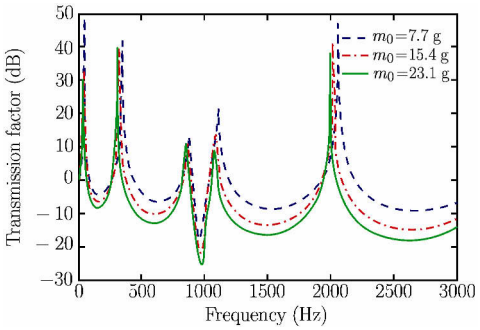

Fig. 7. FRF curves for different concentrated masses.

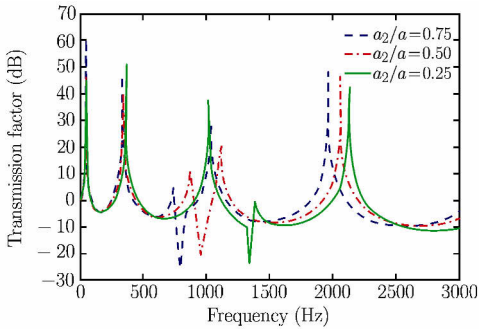

Fig. 8. FRF curves for different width ratios a_2/a.

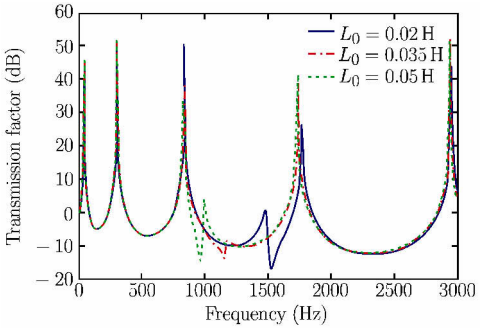

Fig. 9. FRF curves for different inductances of shunt circuits.

Finally, another model of equal frequency circuit is proposed by periodic circuit. The shunt circuits are designed to be periodic. Every inductor in all unit cells has the same inductance. An equal electrode area is needed to make every piezoelectric unimorph own the same equivalent capacitance. Hence width $a_2^{(n)}$ of the nth piezoelectric unimorph should satisfy

$$a_2^{(n)} = R_0 + na - \sqrt{(R_0+na)^2 - 2\,(R_0+a)\,a_2^{(1)} + \left(a_2^{(1)}\right)^2} \tag{44}$$

where $n = 2, 3, \ldots, N$. With the same parameters of $a_2^{(1)} = 10$ mm, $R^{(n)} = 5\,\Omega$, $m_0 = 7.7$ g, $a = 20$ mm, $R_0 = 25$ mm, and $N = 4$ as those in Fig.4, Fig.9 demonstrates that three integrated LR gaps are obtained when the inductances of shunt circuits are $L = 0.02$, 0.035, 0.05 H, respectively. Figure 9 shows the same tendency as Fig.4, i.e. the center frequency of the integrated LR gap decreases with increasing inductance. Compared to those in Fig.4, the piezoelectric unimorphs in Fig.9 have smaller ratios of width, and smaller equivalent capacitance accordingly. Therefore, the integrated LR gaps have larger center frequencies.

IV. CONCLUSIONS

Aiming at the service in a UPMP, a circular thin plate attached periodically by annular piezoelectric unimorphs is proposed to isolate vibration. Two kinds of equal frequency resonant shunt circuits are designed to obtain the LR gap. The theoretical model is verified by the FEM. Bragg BGs doesn't appear in the low frequency region. However, an integrating LR BG is achieved when the resonance frequency of every unit cell is tuned the same. With the increase of the inductance, the frequency of LR BG decreases, and the width of the LR BG becomes narrower. The transmission factor of the LR BG can be reduced dramatically, but the center frequency keeps fixed when the resistance decreases. For LR BG, there exist optimum resistances to obtain a small transmission factor at its center frequency; meanwhile the transmission factors on both sides are not large. The attenuation in VABs is strengthened and the center frequency of these gaps decreases when the concentrated mass increases. Both frequencies of the LR and VABs decrease with increasing material ratio, but with different mechanisms.

References

[1] Wu,B., Wei,R., Zhao,H. and He,C., Phononic band gaps in two-dimensional hybrid triangular lattice. *Acta Mechanica Solida Sinica*, 2010, 23(3): 255-259.

[2] Zhan,Z. and Wei,P., Influences of anisotropy on band gaps of 2D phononic crystal. *Acta Mechanica Solida Sinica*, 2010, 23(2): 181-188.

[3] Liu,Z.Y., Zhang,X.X., Mao,Y.W., Zhu,Y.Y., Yang,Z.Y., Chan,C.T. and Sheng,P., Locally resonant sonic materials. *Science*, 2000, 289(5485): 1734-1736.

[4] Goffaux,C., Sánchez-Dehesa,J., Yeyati,A.L., Lambin,P., Khelif,A., Vasseur,J.O. and Djafari-Rouhani,B., Evidence of Fano-like interference phenomena in locally resonant materials. *Physical Review Letters*, 2002, 88(22): 225502.

[5] Goffaux,C. and Sánchez-Dehesa,J., Two-dimensional phononic crystals studied using a variational method: Application to lattices of locally resonant materials. *Physical Review B*, 2003, 67(14): 144301.

[6] Wang,G., Wang,J., Chen,S. and Wen,J., Vibration attenuations induced by periodic arrays of piezoelectric patches connected by enhanced resonant shunting circuits. *Smart Materials and Structures*, 2011, 20(12): 125019.
[7] Wang,G., Chen,S.B. and Wen,J.H., Low-frequency locally resonant band gaps induced by arrays of resonant shunts with Antoniou's circuit: experimental investigation on beams. *Smart Materials and Structures*, 2011, 20(1): 015026.
[8] Chen,S.B., Wen,J.H., Wang,G., Han,X.Y. and Wen,X.S., Locally resonant gaps of phononic beams induced by periodic arrays of resonant shunts. *Chinese Physics Letters*, 2011, 28: 094301.
[9] Chen,S.B., Wen,J.H., Wang,G., Yu,D.L. and Wen,X.S., Improved modeling of rods with periodic arrays of shunted piezoelectric patches. *Journal of Intelligent Material Systems and Structures*, 2012, 23(14): 1613-1621.
[10] Baz,A., Active control of periodic structures. *Journal of Vibration and Acoustics*, 2001, 123(4): 472-479.
[11] Ruzzene,M. and Baz,A., Active control of wave propagation in periodic fluid-loaded shells. *Smart Materials and Structures*, 2001, 10(5): 893.
[12] Singh,A., Pines,D.J. and Baz,A., Active/passive reduction of vibration of periodic one-dimensional structures using piezoelectric actuators. *Smart Materials and Structures*, 2004, 13(4): 698.
[13] Thorp,O., Ruzzene,M. and Baz,A., Attenuation of wave propagation in fluid-loaded shells with periodic shunted piezoelectric rings. *Smart Materials and Structures*, 2005, 14(4): 594.
[14] Spadoni,A., Ruzzene,M. and Cunefare,K., Vibration and wave propagation control of plates with periodic arrays of shunted piezoelectric patches. *Journal of Intelligent Material Systems and Structures*, 2009, 20(8): 979-990.
[15] Casadei,F., Ruzzene,M., Dozio,L. and Cunefare,K.A., Broadband vibration control through periodic arrays of resonant shunts: experimental investigation on plates. *Smart Materials and Structures*, 2010, 19(1): 015002.
[16] Thorp,O., Ruzzene,M. and Baz,A., Attenuation and localization of wave propagation in rods with periodic shunted piezoelectric patches. *Smart Materials and Structures*, 2001, 10(5): 979.
[17] Casadei,F., Beck,B.S., Cunefare,K.A. and Ruzzene,M., Vibration control of plates through hybrid configurations of periodic piezoelectric shunts. *Journal of Intelligent Material Systems and Structures*, 2012, 23(10): 1169-1177.
[18] Chen,S.B., Wang,G., Wen,J.H. and Wen,X.S., Wave propagation and attenuation in plates with periodic arrays of shunted piezo-patches. *Journal of Sound and Vibration*, 2013, 332(6): 1520-1532.
[19] Shen,Y.P., Chen,X.D., Jiang,W. and Luo,X., Spatial force-based non-prismatic beam element for static and dynamic analyses of circular flexure hinges in compliant mechanisms. *Precision Engineering-Journal of the International Societies for Precision Engineering and Nanotechnology*, 2014, 38(2): 311-320.
[20] Aggogeri,F., Al-Bender,F., Brunner,B., Elsaid,M., Mazzola,M., Merlo,A., Ricciardi,D., de la O Rodriguez,M. and Salvi,E., Design of piezo-based AVC system for machine tool applications. *Mechanical Systems and Signal Processing*, 2013, 36(1): 53-65.
[21] Dai,L.X., Jiang,S., Lian,Z.Y., Hu,H.P. and Chen,X.D., Locally resonant band gaps achieved by equal frequency shunting circuits of piezoelectric rings in a periodic circular plate. *Journal of Sound and Vibration*, 2015, 337: 150-160.
[22] Shu,H.S., Liu,W., Li,S.D., Dong,L.Q., Wang,W.Y., Liu,S.G. and Zhao,D., Research on flexural wave band gap of a thin circular plate of piezoelectric radial phononic crystals. *Journal of Vibration and Control*, 2014, 10.1177/1077546314544694): 1-13.
[23] Yang,J.S., Comment on 'Admittance matrix of asymmetric piezoelectric bimorph with two separate electrical ports under general distributed load'. *IEEE Transactions on Ultrasonics Ferroelectrics and Frequency Control*, 2007, 54(6): 1087-1088.
[24] Wang,Y.J., Lian,Z.Y., Wang,J. and Hu,H.P., Analysis of a piezoelectric power harvester with adjustable frequency by precise electric field method. *IEEE Transactions on Ultrasonics Ferroelectrics and Frequency Control*, 2013, 60(10): 2154-2161.
[25] Yang,J.S., An Introduction to the Theory of Piezoelectricity. Springer, Boston, 2005.
[26] Li,H., Yang,F., Du,H.L., Hu,H.P., Jiang,W., Chen,X.D. and Hu,Y.T., Dynamic characteristics of axially-symmetrical annular corrugated shell piezoelectric transducers. *Acta Mechanica Solida Sinica*, 2009, 22(5): 499-509.
[27] Auld,B.A., Acoustic Fields and Waves in Solids. New York: Wiley, 1973.
[28] Hu,H.P., Hu,Y.T. and Yang,J.S., On the inaccuracy of using Mindlin's first-order plate theory for calculating the motional capacitance of a thickness-shear resonator. *IEEE Transactions on Ultrasonics Ferroelectrics and Frequency Control*, 2009, 56(1): 7-8.